Desalination and Water Treatment
www.deswater.com
doi: 10.5004/dwt.2020.24817

173 (2020) 283–293
January

Removal of spironolactone from aqueous solution using bentonite-supported nanoscale zero-valent iron and activated charcoal

Saleh Sulaiman*,‡, Mohammed Al-Jabari‡

Department of Chemistry, Faculty of Science, Birzeit University, Birzeit, P.O. Box: 14, Ramallah, West Bank, Palestinian Authority, Tel. +970-2-298-2146; Fax: +970-2- 298-2084; emails: ssuliaman@birzeit.edu (S. Sulaiman), maljabari@birzeit.edu (M. Al-Jabari)

Received 15 April 2019; Accepted 25 August 2019

ABSTRACT

The prepared low-cost nano-zero valent iron (nZVI) immobilized on bentonite clay (B) composite was prepared by using the $NaBH_4$ reduction method. The morphology, structure, and composition of prepared B-nZVI was characterized by using scanning electron microscopy, transmission electron microscopy, X-ray diffraction, and UV-Vis spectroscopy. The current study investigates different adsorption and kinetic models that describe the adsorption process of Spironolactone (SP) onto B-nZVI. SP was unstable in both medium of pure water and Birzeit campus activated sludge during the study period. For comparison purposes, the removal of aqueous SP was investigated using activated charcoal and bentonite. The effect of B-nZVI on SP removal was studied at different adsorbent dose, contact time, temperature, pH, and initial SP concentration. The results indicated that B-nZVI is effective in the removal of SP from aqueous solution, where removal efficiency of 99% was achieved after 180 min. for initial SP concentration 100 ± 1.27 mg L^{-1} at pH 7, temperature 30°C and fixed stirring rate 200 rpm. Kinetic studies showed that the removal of SP by B-nZVI correlated well with the pseudo-second-order model. The removal is an endothermic adsorption process, and the experimental data fitted well the Langmuir isotherm with Q_{max} being 111.1 and 125 mg g^{-1} for charcoal and B-nZVI, respectively. The calculated data indicated a significant larger binding affinity of SP by B-nZVI over the charcoal adsorbent.

Keywords: Nanoscale zero-valent iron; Bentonite; Spironolactone; Adsorption; Charcoal

1. Introduction

The occurrence and fate of anthropogenic chemical species, particularly, pharmaceuticals and personal care products in the natural aqueous environment have been attracted much attention from researchers.

Pharmaceuticals compounds are biologically active and found in the environment at trace concentrations [1–4]. It has been recognized as a potential environmental problem [2,3]. Although, the trace concentration levels of pharmaceuticals found in the environment, and their chemical persistence, microbial resistance, specificity, high biological activity, and synergistic effects are still under consideration for further studies [3]. They might cause harm even at lower concentrations than other pollutants detected in the environment, which is a cause of concern in research fields.

Nowadays, nano-zero valent iron (nZVI) particles have received great attention because of their larger specific surface area with a larger number of active intrinsic surface sites, and larger ability in the chemical reduction of recalcitrant substances [5,6].

nZVI particles are liable to react and agglomerate in the adsorption environment, causing a significant decrease in its reactivity [6]. Therefore, various particle-stabilizing

* Corresponding author.

‡ Both authors equally contributed to this work.

methods have been investigated for proficient diffusion of the nZVI particles in a desorption media [7–9].

Recently, carboxymethyl cellulose studied to stabilize nZVI particles for in situ reductive immobilization of Cr(VI) in water [6]. Also, Cr(VI) reduced by using resin-supported nZVI particles in aqueous solution. Reduction of Cr(VI) leads to decrease the removal time to be 20–30 times less than the commercial iron powder per unit mass of Fe dose [6]. Removal efficiently adsorption and low cost of Bentonite (B), has received much potential toward removing of several organic pollutants from an aqueous solution. The Langmuir model was applicable in the adsorption manner of raw B toward these pollutants with B capacity 34.34 mg g^{-1} at pH 4.0 [10,11]. On the other hand, using B as supporting material for nZVI will enhance the removal and degradation efficiency of SP by adsorption on the surface of B-nZVI and reduction by nZVI in aqueous solution.

Sulaiman and Shahwan [4] investigated the behavior and removal efficiency of mefenamic acid, which is a class of non-steroidal, anti-inflammatory drugs. They found that using B-nZVI particles, 42% of mefenamic acid was removed, whereas only 22% by using nZVI after reacting for 10 min. with an initial mefenamic acid concentration of 100 mg L^{-1} (pH = 6) [4].

SP is an artificial, crystalline yellowish solid, is considered as one of the most common pharmaceuticals drug [12,13]. SP, (7α-acetylthio-3-oxo-17α-pregn-4-ene-21, 17-carbolactone) [12,13] (Fig. 1), is a competitive aldosterone antagonist, which is categorized as asteroid drugs. SP is insoluble in water, partially soluble in alcohol, and freely soluble in an organic solvent like benzene and chloroform. It is considered as a potassium-sparing diuretic (water pill) that is used to prevent the body from absorbing too much salt and retain potassium from getting to a dangerously low level. SP has been widely used to treat, allergy, inflammation, and illnesses related to adrenal cortex insufficiency. Also, SP is used to treat or diagnose a condition in which the body has much secretion of aldosterone (hormone regulates the water and salt balance in the human body and produced by adrenal glands) [12–15].

This research focuses on synthesis and characterizations of B-nZVI, the stability and degradation of spironolactone were investigated; and a novel method was described for better removal efficiency of spironolactone by B-nZVI. Kinetic and isotherm Langmuir models were applied, and the obtained experimental data was analyzed. Thermodynamic parameters associated with the adsorption process were calculated.

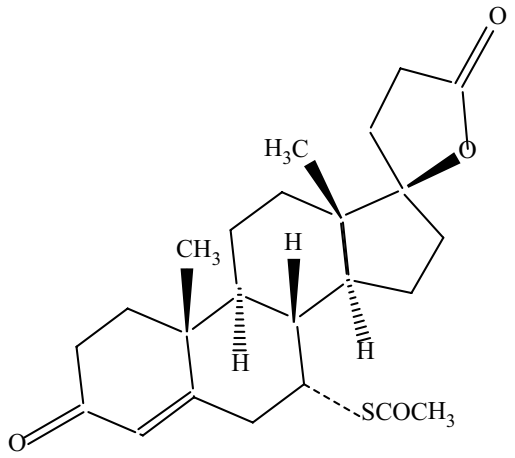

Fig. 1. Structures of spironolactone.

2. Materials and methods

2.1. Chemicals

Bentonite (B) with 32.4 meq/100 g cation exchange capacity, and montmorillonite content (wt.) <40%. The chemical content was 62.5% SiO_2, 18.5% Al_2O_3, 1.75% Fe_2O_3, 4.25% MgO, 2.75% Na_2O and 0.95% CaO. B was sieved with a 200 mesh screen after drying at 30°C for a night before using. Iron chloride hexahydrate ($FeCl_3 \cdot 6H_2O \geq 97\%$), Sodium Borohydride ($NaBH_4 \geq 96\%$) and Spironolactone ($C_{24}H_{32}O_4S \geq 97\%$). Fine powder activated charcoal (particle size ≤ 60 μm) used for batch adsorption experiments, while granular activated charcoal was used in column experiments (particle size ≤700 μm). Spironolactone solution of desired concentration was prepared by dissolving the required amount of the drug in a suitable volume of de-ionized water; the latter used throughout this experiment. De-ionized water was used throughout this experiment. All chemicals used in this study were purchased from Sigma Chemical Company Co. Ltd., (Munich, Germany), and used without further treatment.

2.2. Birzeit University wastewater treatment plant and SP stability

2.2.1. Birzeit University wastewater treatment plant

Birzeit University wastewater treatment plant (WWTP) consists of a contact stabilization bond system, which has been used to treat domestic wastewater from all Birzeit University buildings [4]. Recently, 180 m^3 d^{-1} of sewage collected and treated at Birzeit University from almost 16,000 students and staff [4,16]. The wastewater characteristics from Birzeit University WWTP are slightly diluted and thus do not reflect a typical rural domestic sewage, because most of the students stay for a short period in the university campus [4,16].

2.2.2. Biological, physical, and chemical parameters of Birzeit University WWTP sludge

Before doing any experiments biological, physical and chemical parameters for wastewater used were evaluated according to standard methods [17] listed in Table 1.

2.2.3. Stability study of SP

Stability study for SP presence in the sludge of Birzeit University WWTP performed. It is worth noting, that each experiment performed in triplicate and the average values were recorded. 100 mg L^{-1} was used to test SP stability in both medium, samples were collected at a different time interval, and the SP stability was evaluated by using high-performance liquid chromatography (HPLC).

Table 1
Methods used and wastewater quality parameters measured in the Birzeit University WWTP

Parameter	Instrument	Method	Reference
pH	pH-meter 3320, Jenway (United Kingdom)	SM#4500-H+(B) (on site)	Measurement as manufacturer procedure
Conductivity	Conductivity meter4320, Jenway (United Kingdom)	2520-B	APHA [17]
Total coliforms and fecal coliforms	Membrane filter method	9222-B 9221-E	APHA [17]
Orthophosphate	Ascorbic acid reduction	SM# 4500-PF	APHA [17]
COD	Hach COD reactor (United Kingdom)	5210-B	APHA [17]
BOD_5	DO meter – Oxy 197	5220-D	
NH_4^+	Nesslerization method	4500A-NH_3	APHA [17]
Total bacterial count	Pour plate method	9215D	APHA [17]
Solids	Gravimetric methods	2540B 2540C 2540D	APHA [17]

2.3. Methods

2.3.1. Synthesis of bentonite-supported nZVI

Two types of adsorbent were synthesized; nZVI nanoparticles and bentonite-nZVI via liquid-phase reduction method in which bentonite acted as a support material as mentioned formerly [4,8,18]:

$$4Fe^{3+} + 3BH_4^- + 9H_2O \rightarrow 4Fe^0 + 3H_2BO_3^- + 12H^+ + H_2\uparrow \quad (1)$$

B-nZVI was synthesized in (1:1) mass ratio of Fe^0 and B, where 9.68g of $FeCl_3{\cdot}6H_2O$ was dissolved in 100 mL of pure ethanol and bi-distilled water of volume ratio (4:1), followed by addition of 2.00 g of B. The mixture was kept continuously mixing in three-neck flask for 15 min in an inert atmosphere of nitrogen gas. Then, 200 ml of 0.47 M $NaBH_4$ solution was gradually added to the mixture at the rate of 1–2 drops per second, the mixture kept vigorously and continuously stirred under an inert atmosphere. The mixture's color gradually converted from red-brown to light yellow then to black, and simultaneously, the mixture formed black particles during the reaction process [4,19].

After the complete addition of the $NaBH_4$ solution, the mixture was kept stirred continuously for an additional 30 min under an inert atmosphere to complete consuming $NaBH_4$ and $FeCl_3{\cdot}6H_2O$. After that, the B-nZVI particles were collected using vacuum filtration, and quickly rinsed and washed three times by absolute ethanol. The produced B-nZVI was dehydrated overnight at 333 K under vacuum, and to avoid oxidation of nZVI the samples were kept retained as a powder in a nitrogen atmosphere for further study and analysis [20].

2.3.2. Sample characterizations

IR spectra were acquired via a Fourier transform infrared spectroscopy (FTIR-Nicolet 5700, Thermo Corp., USA). The tested solution was directly analyzed using attenuated total reflectance-Fourier-transform infrared. Five scans for each sample were done and the average was taken with a resolution of 4 cm^{-1} [4].

The morphology and nanoparticles distribution of nZVI on bentonite surface were analyzed by using a Philips-FEI XL30 ESEM-TMP (Philips Electronics Co., Eindhoven, Netherlands). The images of samples were recorded at different magnifications at an operating voltage of 20 kV [4].

X-ray diffraction (XRD) patterns of B-nZVI samples was recorded using a Philips-X'Pert Pro MPD (Netherlands) instrument with a high-power Cu Kα source (K = 0.154 nm) at 40 kV and 40 mA. All samples were measured at the diffraction angle range of 2θ = 5°–90° at a scanning rate of 3°min^{-1} [4].

Analyses were performed by an alliance 2695 HPLC (Waters: Milford, MA, USA), consist detector with photodiode array of waters Micromass® Masslynx™ (Waters 2996). Data were recorded and analyzed using Empower™ software (Waters). A conjugated of two columns were used to separate the analytes, BXridge™ C18 guard column (4.6 mm × 20 μm) conjugated with (4.6 mm × 150 mm) C18 X Bridge® column (5 μm particle size). Microfilter of 0.45 μm was used (Acrodisc® GHP, Waters, USA).

2.3.3. Batch experiments

To study the efficiency of both adsorbent B-nZVI and AC toward SP removal, several solutions with different SP initial concentration were prepared: 100 ml from each solution poured into a 250 mL Erlenmeyer flask (Darmstadt, Germany), then adding 0.1 g of the adsorbent to each flask, separately. Solutions were shaken for 180 min, and the effect of contact time was studied for 100 mg L^{-1} SP concentration at 30°C. The samples were collected and analyzed at different time intervals. Also, the adsorbent concentration in the range of 0.1–1.0 g L^{-1} was studied, and the effect of temperature in the range of 15°C–55°C was evaluated.

At the end of the contact periods, each sample was filtered via 0.45 μm filters. In each case, a volume of 20 μL filtered sample was injected into the HPLC and the respond of SP was recorded. The percentage removal of SP concentration

was calculated by using the well-known mass balance equation:

$$R(\%) = \frac{C_0 - C_t}{C_0} \times 100\% \quad (2)$$

where R (%) is the percentage removal, C_0 (mg L^{-1}) is the initial liquid concentration of SP, and C_t (mg L^{-1}) is the liquid concentration of SP at a specific time t.

3. Results and discussion

3.1. Wastewater characteristics and stability of SP

Table 2 summarizes the chemical, physical, and biological characteristics of wastewater collected from the Birzeit University WWTP aeration tank. Careful assessment of Table 2 shows that the sludge is rich in nutrients with medium values of total dissolved solids (TDS), chemical oxygen demands, biological oxygen demands, settable solids, and high bacterial count. The results are predictable because the tested samples were collected from the aeration tank unit within the WWTP. Results also demonstrated that wastewater used in the current experiment contains medium amounts of suspended solids and large populations of bacteria. Previous analysis of Birzeit University activated sludge reported presence of *Enterobacter* species: *Enterococcus faecalis*, *Enterobacter sakazakii*, *Escherichia coli*, *Pseudomonas aeruginosa*, *Enterobacter aerogenes*, *Klebsiella pneumonia*, *Enterobacter cloacae*, *Salmonella* spp., *Pseudomonadaceae*, *Comamonadaceae*, *Flavobacteriaceae*, *Verrucomicrobiaceae*, *Enterobacteriaceae*, *Staphylococcus aureus*, *Streptococcus*, *Neisseriaceae*, *Enterococci* and *Leptotrichiaceae* [4]. Additionally, high values of TDS and electrical conductivity are expected in municipal wastewaters, but these values can be regulated if WWTP effluents are going to be reused for crop irrigation.

SP stability was monitored in pure water and Birzeit University sludge using 100 mg L^{-1} SP concentration. The collected data from both medium showed that the SP was unstable and exposure to water hydrolysis and rapid bacterial degradation [21].

Previous studies monitored the substances produced from the biodegradation of SP. The results referred that the SP is decomposed into two metabolites [12,22]. Pramar et al. [12,23] who proposed the mechanism of SP degradation to canrenone by several of known reaction in which SP converted to unknown products passing through canrenone. The human body is expansively metabolized of SP since around 79% of the SP oral dose is decomposed to canrenone, which is the major biologically active metabolite [12,23]. Furthermore, hydrolysis for γ-lactone rings of canrenone to produce a water-soluble canrenoic acid (CA). Therefore, after equilibrium, a similar concentration of canrenone and plasma of CA are existed [24]. The previous study of liquid chromatography–mass spectrometry metabolites analysis indicates the absence of sodium and potassium [12], while other evidence from in vitro studies suggested that potassium canrenoate one of the principal active metabolite analogs [12,24,25].

3.2. nZVI characterization

Typically, iron oxide forms are thermodynamically stable, while nZVI is unstable and oxidized very easily in the presence of oxygen. The high chemical reactivity of metallic iron particles leads to its high capability in transforming different contaminants to less toxic forms [4,26,27].

nZVI is well-known to reveal a typical core-shell structure, which forms of zero-valent or metallic iron (Fe^0), while the shell is formed as a result of oxidation of the nanoparticles and composed of mixed valent iron [Fe(II) and Fe(III)] oxides. Also, the research results showed that nZVI possesses especial electron donating characteristics, which makes it a resourceful remediation substance [28]. Through its core-shell structure, nZVI can fix the contaminants by a redox mechanism and/or a sorption mechanism. The core forms an electron source for the redox reactions with several types of organic and inorganic pollutants, while the oxide shell offers the sites for chemisorption [4].

Since ZVI nanoparticles have strong magnetic dipoles, it forms chain-like aggregates. When the nanoparticles agglomerate, have a permanent oxide shell but thinner interfacial oxide layers separate the metallic cores. The iron oxide layer is amorphous and disordered characteristic, causing to the extremely small radii of the nanoparticles, which hinders the crystalline formation and protects the core of the nanoparticles against further oxidation [4,29,30].

The core layer plays an important role in the charge transfer from the nanoparticle core to the sequestrated contaminant on the external surface [4]. It has semiconductor

Table 2
Physical, chemical and biological parameters of used wastewater

Parameters	Results	Parameters	Results	Units
pH	7.82 ± 0.02	TSS	730 ± 20	mg L^{-1}
Conductivity μSm cm^{-1}	532 ± 10	BOD	170 ± 50	mg L^{-1}
Temperature, °C	16.5 ± 0.3	COD	380 ± 50	mg L^{-1}
Turbidity, NTU	5,200 ± 300	NH_4–N	19.7 ± 0.5	mg L^{-1}
DO, mg L^{-1}	1.21 ± 0.02	PO_4-P	4.8 ± 0.4	mg L^{-1}
TS, mg L^{-1}	1,280 ± 30	FC (*E. coli*)	$3.3 \times 10^5 \pm 1.7 \times 10^5$	cfu/100 mL
TDS, mg L^{-1}	362 ± 30	TC	$4.2 \times 10^6 \pm 3.3 \times 10^6$	cfu/100 mL
Settable solids, mg L^{-1}	220 ± 10	TAC	$1.8 \times 10^7 \pm 1.6 \times 10^7$	cfu/100 mL

DO: dissolved oxygen; TS: total solids; TDS: total dissolved solids; TSS: total suspended solids; TAC: total aerobic count.

properties [4,31,32], and its charge transfer is relatively shallow due to small thickness and the presence of not working sites which can assist the reduction of pollutants to take place [31,32].

nZVI and B-nZVI used in this study were characterized using XRD, scanning electron microscopy (SEM), transmission electron microscopy (TEM) and FTIR. The XRD spectra are shown in Fig. 2. The occurrence of nZVI in the sample is marked by the basic reflection at 45°. The nZVI samples usually suffer from low crystallinity, which is due to the presence of boron (originating from the reducing agent $NaBH_4$) in the lattice of the metal nanoparticles. The figure also shows the reflections of montmorillonite (*M*) – the main component of bentonite – in addition to quartz (*Q*) which exists as an impurity in the bentonite sample. The montmorillonite reflections disappeared from the XRD diagram of B-nZVI, possibly indicating that the clay experienced exfoliation upon incorporating Fe nanoparticles in-between its layers. Fig. 2 also provides an XRD pattern of nZVI after the removal of aqueous SP. The sample has undergone massive oxidation as evident by the disappearance of Fe^0 reflection and the appearance of Fe_3O_4 (magnetite) reflections.

SEM images of a fresh sample of nZVI, B-nZVI, and bentonite are demonstrated in Fig. 3. Raw bentonite appears as large flocs with leafy-like lamellas and plenty of small ravines among different interlaminations as shown in Fig. 3a. On the other hand, Figs. 3b and c show that synthesized nZVI possesses typical chain-like aggregates, composed of spherical nanoparticles.

In B-nZVI, a partial decrease in the aggregation of the nanoparticles seems to occur and the aggregated and dispersed nanoparticles seem to accumulate at the internal structure of the clay [4]. Fig. 3d demonstrates that nZVI morphology has largely changed suggesting that the material undergoes massive oxidation after the removal of the contaminant, which confirmed by XRD results given above [4].

The limited diffusion of nZVI on bentonite sheets is clear in the TEM image shown in Fig. 4. The average size of individual nZVI distributed on bentonite structure seems to vary in the range of 40–100 nm [4].

The FTIR spectra of Bentonite and B-nZVI investigated before and after adsorption of SP over a range of 400–4,000 cm^{-1} (Fig. 5). The vibration band at 915 cm^{-1} related

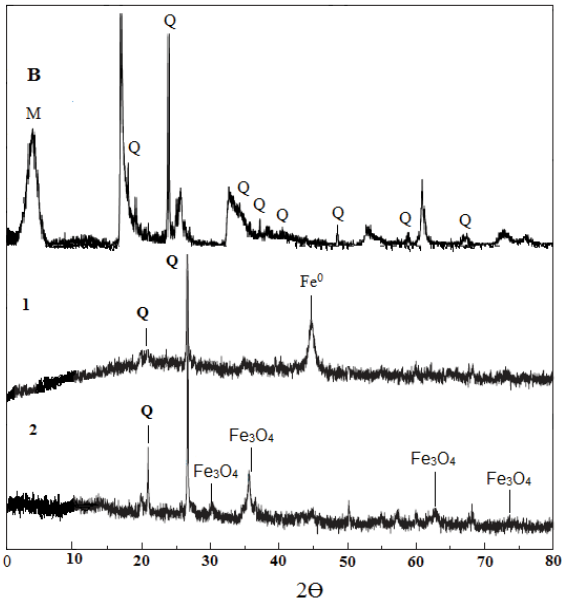

Fig. 2. XRD patterns: (B) bentonite; (1) B-nZVI before adsorption and (2) B-nZVI after adsorption.

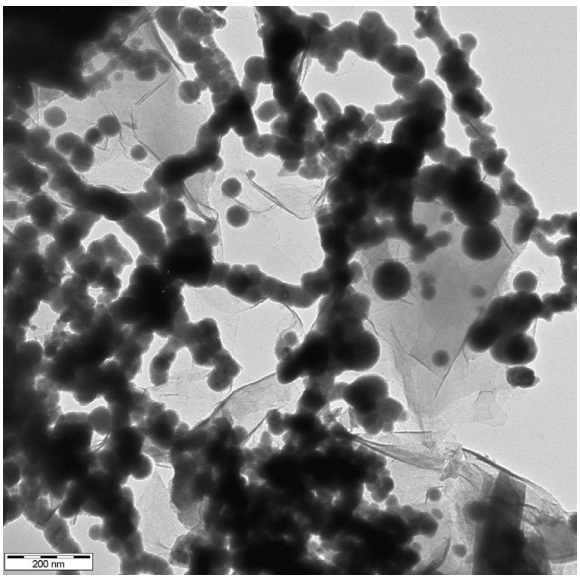

Fig. 4. TEM image of B-nZVI.

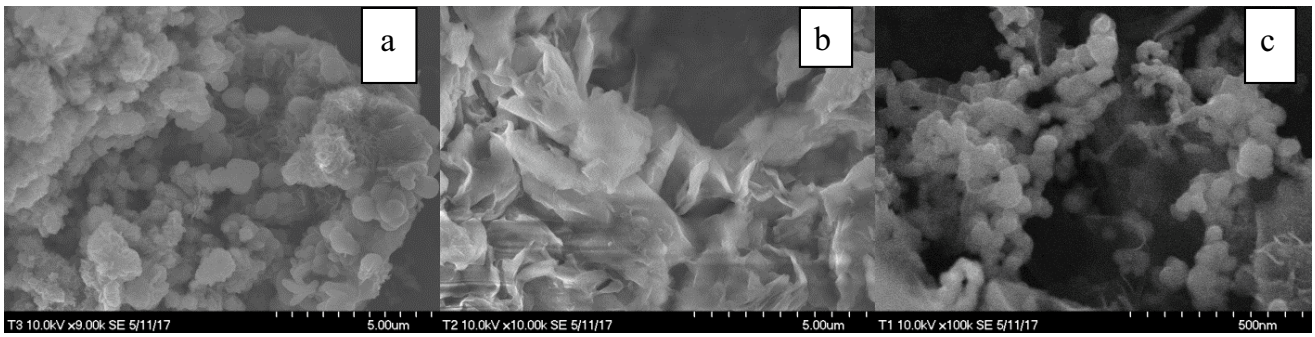

Fig. 3. SEM images of several substances: (a) B, (b) nZVI before adsorption, and (c) B-nZVI after adsorption.

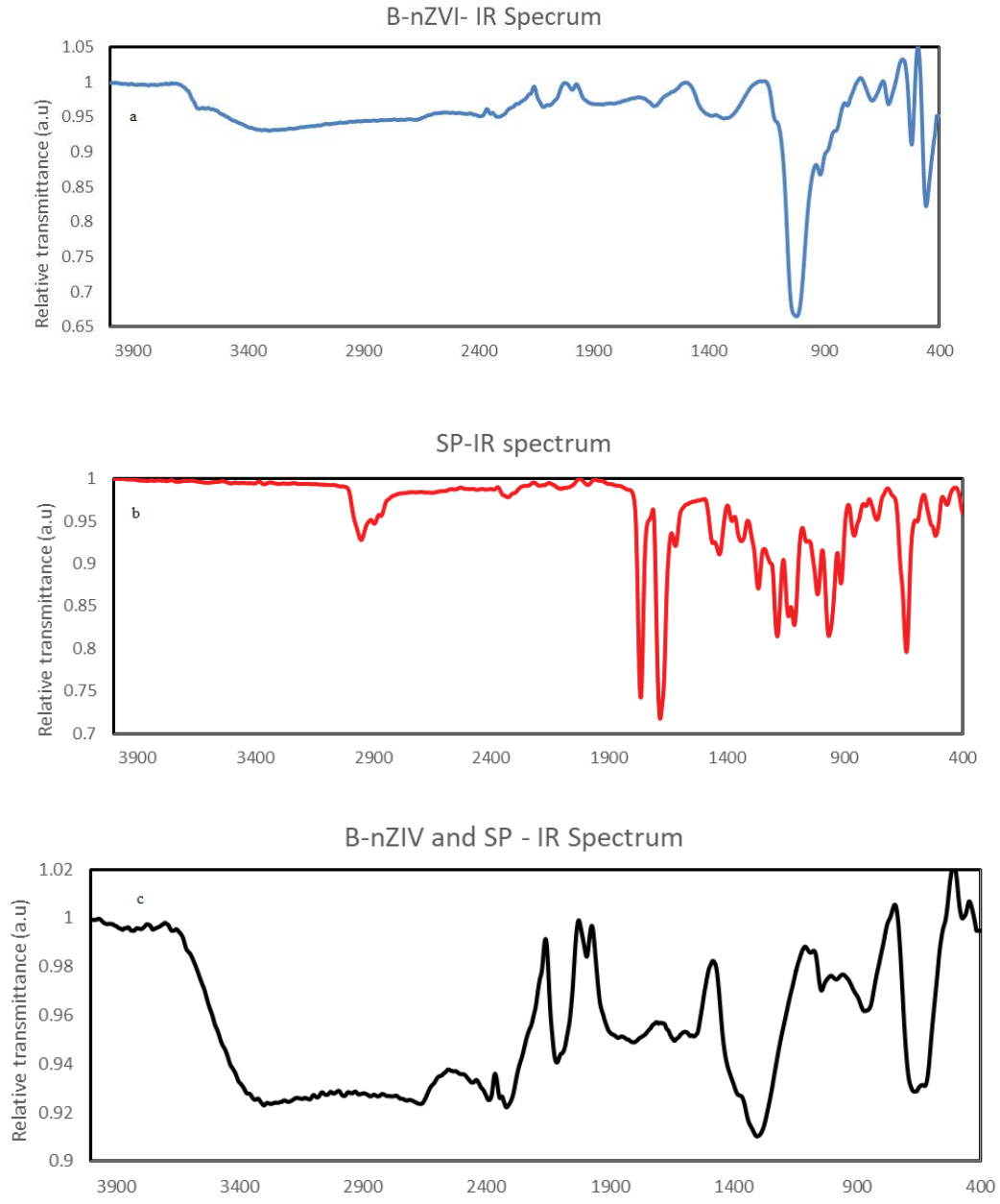

Fig. 5. FTIR spectra of: (a) B-nZVI, (b) SP, and (c) B-nZVI and SP after adsorption.

to Al–O bond, while the band at 3,626 cm^{-1} indicates the presence of Al–O–H groups. Si–O vibrations band occurs at 1,020 cm^{-1}. The two bands at 437 and 520 cm^{-1} are referring to Si–O–Si and Si–O–Al (octahedral) bending vibrations, respectively [4,33,34]. The stretching deep band of Si–O bond in the Si–O–Si group of the tetrahedral sheet appears at 1,018 cm^{-1}. The stretching vibration bands of H–O–H water molecule that hydrogen-bonded to the Si–O surface in B shown at 1,638 cm^{-1}. Also, the bands at 458, 519, 797, 915, and 1,020 cm^{-1} refer to the Fe–O stretching which is originating from the thin layer of iron oxide [4,33]. These results are consisting well with oxide bands that appeared in B-nZVI spectrum which confirms partial oxidation for nZVI in B-nZVI. No new band appeared after B-nZVI was reacted with SP. This is probably because most of the adsorbed SP concentration (or the concentration of its degradation products) is below the limit of detection of the FTIR instrument.

3.3. Comparative removal efficiency of SP by different substances

3.3.1. Effect of time

Fig. 6 represents the removal efficiency of SP from 1,000 mL of an aqueous solution of 100 mg L^{-1} initial concentration by using conventional adsorbents B, activated

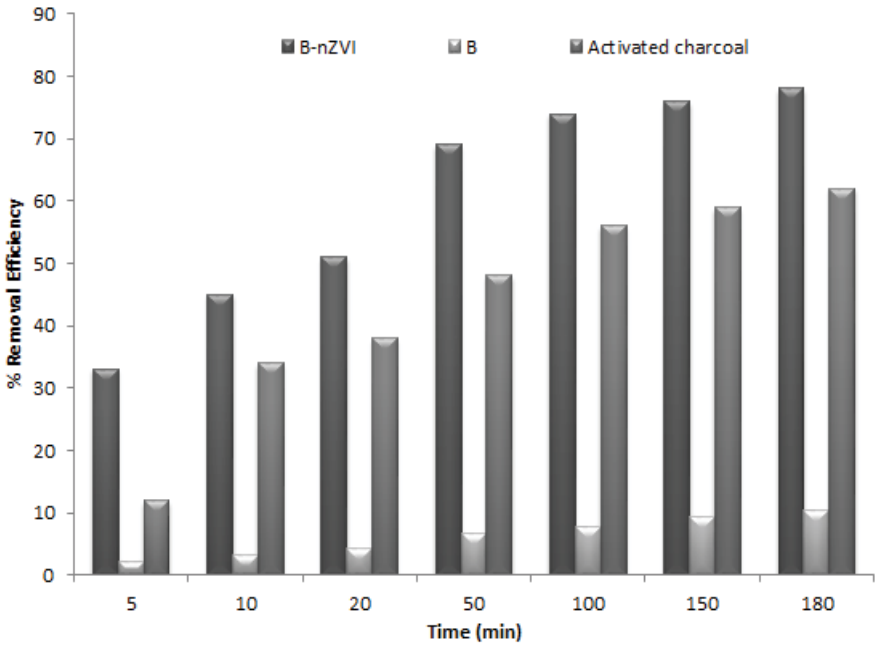

Fig. 6. Percentage removal of SP from dispersions by B-nZVI (■), activated charcoal (■), and bentonite (■) as a function of time, C = 100 mg L^{-1}, dose = 0.1 g L^{-1}, and T = 30°C.

charcoal, and the synthesized B-nZVI. The results showed that B-nZVI is the best performance with a maximum removal efficiency of 80%, followed by charcoal, and finally bentonite, which showed very low removal efficiency. Also, the data indicate that about 1 h is the time needed to approach equilibrium when B-nZVI is used. Given the high removal capacity of B-nZVI toward SP, this confirms that the B established a good dispersibility and suspensibility for nZVI during SP adsorbing process [4] and it improved the reactivity of B-nZVI complex [4,35] with limited sorption efficiency toward SP [36–39].

Bentonite seems to be acting mainly as a dispersant of nZVI, which reliable with previous studies results obtained for kaolin-supported nZVI and bentonite-supported nZVI in the removal of Cr(V) [38], and Pb(II) from aqueous solution [37].

The kinetic data of SP removal by B-nZVI and activated charcoal tested using a modified pseudo-second-order rate equation, given as [40]:

$$\frac{t}{Q} = \frac{1}{Q_m C_0 k_2} + \frac{1}{Q_m} t \tag{3}$$

where Q_m is the maximum amount of the adsorbate, C_0 is the initial concentration, and k_2 is the rate constant. Both Q_m and k_2 obtained from the slope and the intercept of the linear plots of t/Q vs. t.

The linear plots of the data are given in Fig. 7 for SP removal by B-nZVI and charcoal. Under the specified conditions, the obtained values of Q_m are 28.60 mg g^{-1} for B-nZVI and 24.4 mg g^{-1} for charcoal, while the k_2 values are 7.3 × 10^{-4} L min^{-1} mg and 4.6 × 10^{-4} L min^{-1} mg^{-1}, respectively. These calculated values suggest that B-nZVI has a higher removal capacity of SP than charcoal and that the removal process is faster in the case of B-nZVI.

3.3.2. *Effect of initial concentration*

The removal of SP at several initial concentrations by B-nZVI, bentonite, and activated charcoal was investigated. Table 3 summarizes the percentage removal of SP using B-nZVI, bentonite, and activated charcoal. Under the specified conditions, B-nZVI showed the best performance at different initial concentrations, while bentonite showed very low removal percentages, thus suggesting that nZVI is the complex component responsible for the pragmatic removal of SP [4]. However, based on the three types of adsorbents, it is clear that under the same experimental conditions, the proportion removal of SP increased as the initial concentration was increased. The experimental data were evaluated using Langmuir isotherm, which is given by equation [3]:

$$\frac{C_e}{Q_e} = \frac{1}{\left(k\, Q_{\max}\right)} + \frac{C_e}{Q_{\max}} \tag{4}$$

Here C_e (mg L^{-1}) is equilibrium concentration of SP, Q_e (mg g^{-1}) is equilibrium mass of adsorbed SP per gram of sorbent, k (L mg^{-1}) is Langmuir binding constant, and $Q_{\max}$ (mg g^{-1}) is a maximum mass of drug removed per gram of adsorbent.

Experimental data show that decreasing of SP concentration by B-nZVI and activated charcoal were found to fit the Langmuir isotherm model (Eq. (3)), with R^2 being more than 0.98 for both models (Fig. 8). The Langmuir constants ($Q_{\max}$ and k) were valuated and offered in Table 4 [4]. The inspection of Table 4 reveals that the data fitted well the

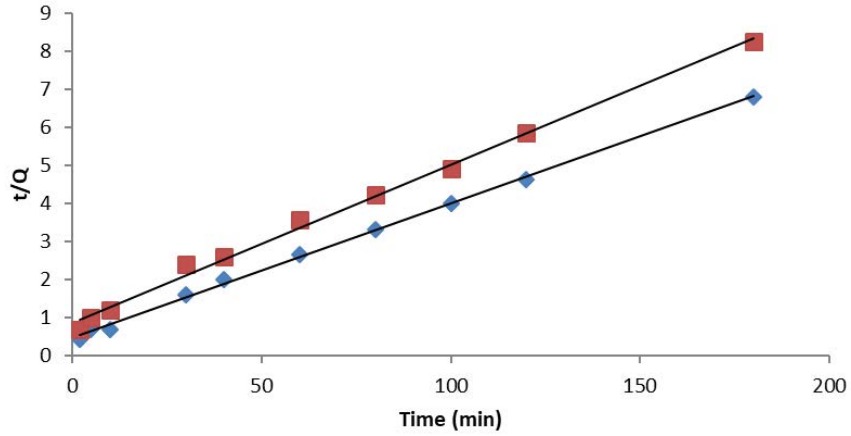

Fig. 7. Kinetic plots of SP removal by B-nZVI (◆) and activated charcoal (■) using a modified pseudo-second-order equation.

Table 3
Percentage removal of SP by B-nZVI, bentonite, and activated charcoal as a function of initial concentration after incubation for 3 h at a temperature of 30°C, B-nZVI dose 0.1 g L^{-1}

SP concentration (mg L^{-1})	Percentage removal (%) initial concentration		
	B-nZVI	Bentonite	Activated charcoal
5	34 ± 0.5	1.4 ± 1	12 ± 0.5
10	45 ± 0.6	1.8 ± 1	34 ± 0.5
20	52 ± 1	3.5 ± 1	48 ± 1
50	69 ± 1	3.9 ± 1	56 ± 1
100	76 ± 1	4.8 ± 1	69 ± 1
200	84 ± 1	5.6 ± 1	72 ± 1

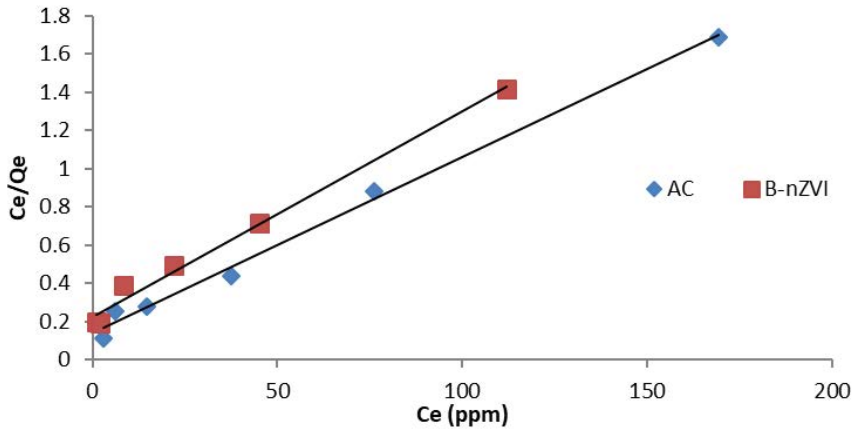

Fig. 8. Langmuir isotherms for the removal of SP by B-nZVI (■) and activated charcoal (◆) at pH 7.0, and 30°C.

Langmuir equation giving $R^2 = 0.9895$ for charcoal and 0.9984 for the B-nZVI (Fig. 8). Langmuir constants Q_{max} and k were determined from the slope and intercept in Fig. 8. B-nZVI has larger k and Q_{max} than activated charcoal. The Langmuir binding constant (k) for the B-nZVI complex was about 1.5-fold greater compared with the activated charcoal, and the value of Q_{max} was nearly 1.2-fold higher for the former. Therefore, in terms of removal capacity and affinity; B-nZVI is more efficient synthesized material for removal of SP than the other tested adsorbents, [4].

3.3.3. Effect of B-nZVI concentration

The consequence of SP removal was investigated with various doses of B-nZVI, namely 0.1, 0.25, 0.5, 0.75, and 1.0 g L^{-1}. The corresponding removal percentages are shown

in Fig. 9a. The data indicates that the dose of 0.25 g L^{-1} B-nZVI would be enough to achieve a complete drug removal under the considered conditions. Beyond this amount, the percentage removal did not change which suggested the availability of enough surface sites that produced a complete removal of SP [4]. A further test for the effect of adsorbate dose was investigated by synthesized B-nZVI. The experiments were conducted at higher SP initial concentrations, namely 50, 100, 300, 500, and 1,000 mg L^{-1} while increasing the sorbent loading to 0.25 g L^{-1}. The results are shown in Fig. 9b indicates that up to 100 mg L^{-1} SP concentration, a complete removal is achievable. Beyond this, the percentage removal decreases as initial concentration increases. This trend is the opposite of the results were observed at a lower concentration range given above and underlines the importance of the concentration range on the extent of SP removal. The indicated results at high initial concentrations of SP can be attributed to the unavailability of an adequate number of active sites since a fixed amount of sorbent concentration was used [4,41].

Table 4
Langmuir isotherm parameters (k and Q_{max}) and the correlation coefficient (R^2) values obtained from the removal of SP on B-nZVI and activated charcoal

Adsorbents	Langmuir		
	k (L mg^{-1})	Q_{max} (mg g^{-1})	R^2
B-nZVI	0.0769	125.0 mg g^{-1}	0.9984
Charcoal	0.0557	111.1 mg g^{-1}	0.9895

3.3.4. Temperature Effect

The effect of temperature on the SP removal by B-nZVI was investigated in the range of 20°C–55°C. Fig. 9c shows that the increase in temperature increased the removal of SP from 74.0% at 20°C to 100.0% at 30°C. Beyond this temperature, the removal appears to stay almost complete. This endothermic behavior indicates that the temperature increases the chemical potential of SP molecules in the solution, thus increasing their mobility and yielding a complete removal.

3.3.5. pH Effect

To study pH effect on SP removal effectiveness by B-nZVI adsorbent, 0.25 g L^{-1} of B-nZVI adsorbent was added on various SP solutions of different pH ranging from 3.0 to 9.0

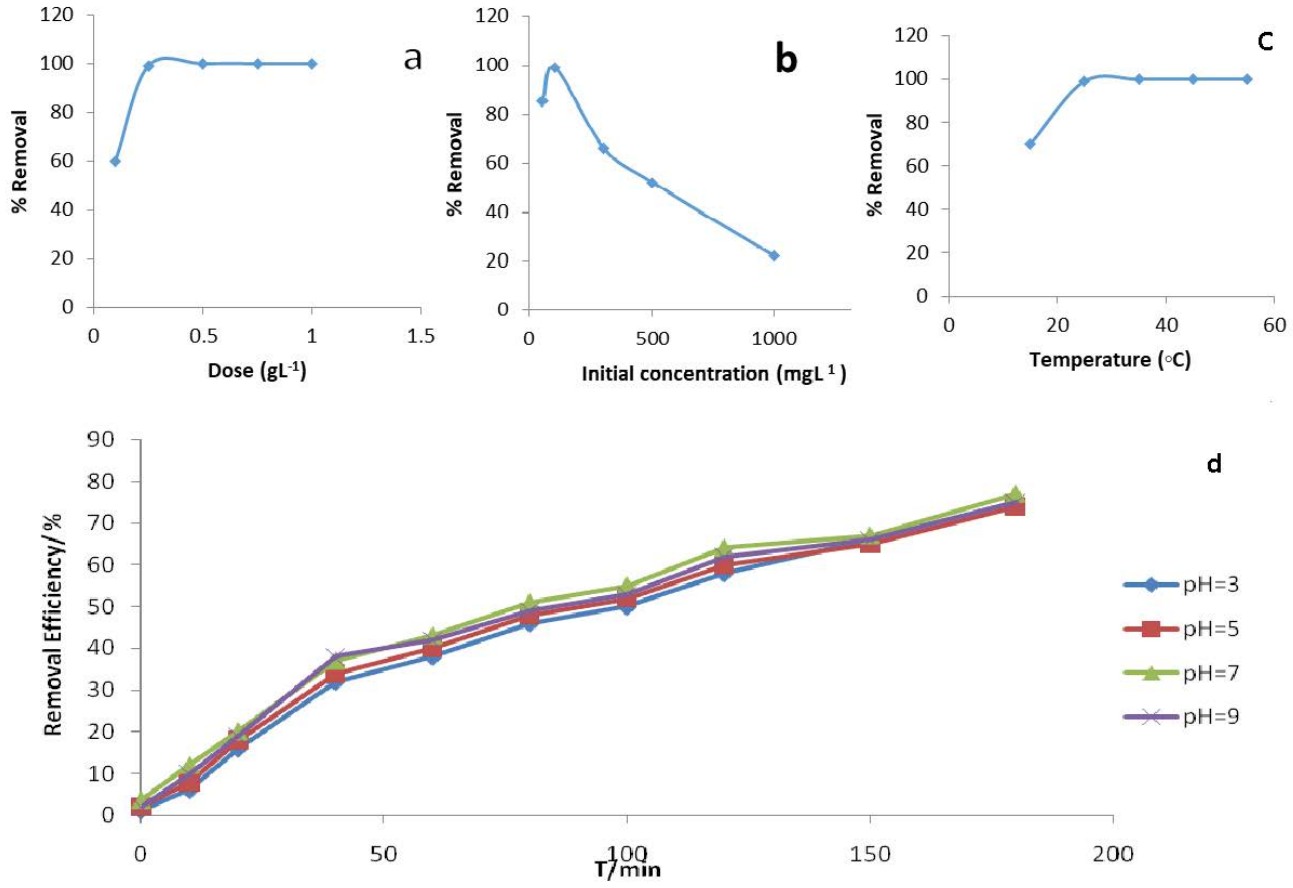

Fig. 9. Conditions affecting the adsorption of SP: (a) effect of B-nZVI dose, (b) effect of SP initial concentration, (c) effect of temperature, and (d) effect of pH.

at 30°C, at an initial 100 mg L^{-1} SP concentration. As shown in Fig. 9d, the SP elimination concentration decreased as the pH values changed from 3.0 to 9.0, and after 180 min, almost 100% of SP was removed by B-nZVI adsorbent. However, when pH decreases the rate of SP removing increases, this can be explained by ionization of nZVI surface and deprotonating of SP. Also, the presence of the thioester group in SP adsorbate can undergo hydrolysis easily, while the presence of H^+ at low pH encourages the formation of Fe(II)–SP complex by the reduction of SP [41]. This leads to enhancing the adsorption removal of SP by the surface of B-nZVI adsorbent [42,43]. In contrast, at high pH values, the hydroxide precipitation was observed, which caused a blocking for the active surface sites by forming a shell over nZVI and reducing the decomposition of SP. The results are also consistent with another previous study which indicates the formation of maghemite (γ-Fe_2O_3) and magnetite (Fe_3O_4) during the preparation of B-nZVI, which was established by SEM images and XRD [43,44].

The PZC of bentonite, nZVI, fresh B-nZVI and recovered B-nZVI was 3.5, 8.6, 7.3 and 5.2, respectively. As can be seen, the PZC of B-nZVI is larger than that of bentonite which was due to the evenly disperse of nZVI, this facilitated the anionic contaminants adsorbed on B-nZVI. After several runs, the PZC of B-nZVI decreased compared with fresh B-nZVI, the main reason was the consumption of nZVI during the electrolysis process. Saturated adsorption of cationic contaminants on B-nZVI might be another reason [45,46].

4. Conclusions

Iron nanoparticles employed in this research consisted mainly of zero-valent Iron. It has been observed that B can act as a stabilizer and dispersant for nZVI particles during B-nZVI synthesis, causing to reduce the aggregation and improved activity of nZVI. SP was unstable in both distilled water and Birzeit University sludge during the study period. Batch experiments applied different parameters such as adsorbent dosage the initial concentration of SP, time, temperature and pH have various effects on the adsorption process, but complete removal of the drug is possible under a wide range of conditions. The obtained data correlated well with the pseudo-second-order rate equation and Langmuir isotherm. The comparative study of B-nZVI and activated charcoal indicated that the B-nZVI possesses higher removal capacity and faster removal kinetics. The removal mechanism of SP using B-nZVI may be proposed by adsorption and redox routes, which lead to adsorption of SP to B-nZVI, the formation of Fe(II)-SP complex, and/or cleavage of SH bond of SP. However, further studies are required to shed more light on the removal mechanism. Overall, the results suggest that the incorporation of B-nZVI filters in secondary WWTPs could be promising in removing SP from the aquatic environment.

Acknowledgments

The financial support for this research from the Scientific Research Committee at Birzeit University is gratefully acknowledged. We thank our colleagues from Birzeit University: Assem M. Mobarak, Azmi N. Dudin, and Shadi H. Kaibni for their technical support that greatly assisted the research. The authors thank Montaha Masri (Ulm University) for her assistance in the XRD, SEM, and TEM characterization of iron nanomaterials.

References

[1] C.G. Daughton, Non-regulated water contaminants: emerging research, Environ. Impact Assess. Rev., 24 (2004) 711–732.
[2] C.G. Daughton, T.A. Ternes, Pharmaceuticals and personal care products in the environment: agents of subtle change?, Environ. Health Perspect., 107 (1999) 907–937.
[3] K. Kummerer, Present Knowledge and Need for Further Research, In: Pharmaceuticals in the Environment, Springer Verlag, Heidelberg, 2001, pp. 239–245.
[4] S. Sulaiman, T. Shahwan, Mefenamic acid stability and removal from wastewater using bentonite-supported nanoscale zero-valent iron and activated charcoal, Desal. Wat. Treat., 97 (2017) 175–183.
[5] J. Theron, J.A. Walker, T.E. Cloete, Nanotechnology and water treatment: applications and emerging opportunities, Crit. Rev. Solid State, 34 (2008) 43–69.
[6] X.-q. Li, D.W. Elliott, W.-x. Zhang, Zero-valent iron nanoparticles for abatement of environmental pollutants: materials and engineering aspects, Crit. Rev. Solid State, 31 (2006) 111–122.
[7] S.M. Ponder, J.G. Darab, T.E. Mallouk, Remediation of Cr(VI) and Pb(II) aqueous solutions using supported, nanoscale zero-valent iron, Environ. Sci. Technol., 34 (2000) 2564–2569.
[8] T. Shahwan, Ç. Üzüm, A.E. Eroglu, I. Lieberwirth, Synthesis and characterization of bentonite/iron nanoparticles and their application as adsorbent of cobalt ions, Appl. Clay Sci., 47 (2010) 257–262.
[9] Ç. Üzüm, T. Shahwan, A.E. Eroglu, K.R. Hallam, T.B. Scott, I. Lieberwirth, Synthesis and characterization of kaolinite-supported zero-valent iron nanoparticles and their application for the removal of aqueous Cu^{2+} and Co^{2+} ions, Appl. Clay Sci., 43 (2009) 172–181.
[10] E. Eren, Adsorption performance and mechanism in binding of azo dye by raw bentonite, CLEAN – Soil Air Water, 38 (2010) 758–763.
[11] V.K. Gupta, Suhas, Application of low-cost adsorbents for dye removal – a review, J. Environ. Manage., 90 (2009) 2313–2342.
[12] S. Sulaiman, M. Khamis, S. Nir, F. Lelario, L. Scrano, S.A. Bufo, R. Karaman, Stability and removal of spironolactone from wastewater, J. Environ. Sci. Health., Part A, 50 (2015) 1127–1135.
[13] V. Laurian, I. Silvia, M. Dana, A. Marcela, M. Daniela-Lucia, Determination of spironolactone and canrenone in human plasma by high-performance liquid chromatography with mass spectrometry detection, Croat. Chem. Acta, 84 (2011) 361–366.
[14] S.A. Doggrell, L. Brown, The spironolactone renaissance, Expert Opin. Invest. Drugs, 10 (2001) 243–254.
[15] S.J. Lloyd, V.F. Mauro, Spironolactone in the treatment of congestive heart failure, Ann. Pharmacother., 34 (2000) 1336–1340.
[16] R. Al-Saed, O. Zimmo, Process performance evaluation of the contact stabilization system at Birzeit University, Int. J. Environ. Pollut., 21(2004) 511–517.
[17] American Public Health Association, Standard Methods for the Examination of Water and Wastewater, 21st ed., APHA, Washington, D.C., USA, 2005.
[18] M. Rafatullah, O. Sulaiman, R. Hashim, A. Ahmad, Adsorption of methylene blue on low-cost adsorbents: a review, J. Hazard. Mater., 177 (2010) 70–80.
[19] H.j. Kim, H.-J. Hong, Y.-J. Lee, H.-J. Shin, J.-W. Yang, Degradation of trichloroethylene by zero-valent iron immobilized in cationic exchange membrane, Desalination, 223 (2008) 212–220.
[20] J.J. Zhan, T. Zheng, G. Piringer, C. Day, G.L. McPherson, Y.F. Lu, K. Papadopoulos, V.T. John, Transport characteristics of nanoscale functional zerovalent iron/silica composites for in situ remediation of trichloroethylene, Environ. Sci. Technol., 42 (2008) 8871–8876.

[21] G.D. Champion, G.G. Graham, Pharmacokinetics of non-steroidal anti-inflammatory drugs, Aust. N. Z. J. Med., 8 (1978) 94–100.
[22] United States Environmental Protection Agency (USEPA), Wastewater Treatment Manuals: Primary, Secondary and Tertiary Treatment, Author: Washington, D.C., 1997.
[23] Y. Pramar, V.D. Gupta, T. Zerai, Quantitation of spironolactone in the presence of canrenone using high-performance liquid chromatography, Drug Dev. Ind. Pharm., 17 (1991) 747–761.
[24] D.-M. Huang, T.-Z. Zhang, F.-J. Cui, W.-J. Sun, L.-M. Zhao, M.-Y. Yang, Y.-J. Wang, Simultaneous identification and quantification of canrenone and 11-α-hydroxy-canrenone by LC-MS and HPLC-UVD, J. Biomed. Biotechnol., 2011 (2011) 7 p, doi: 10.1155/2011/917232.
[25] L.E. Ramsay, J.R. Shelton, D. Wilkinson, M.J. Tidd, Canrenone-the principal active metabolite of spironolactone, J. Clin. Pharmacol., 3 (1976) 607–612.
[26] C. Noubactep, S. Caré, R.A. Crane, Nanoscale metallic iron for environmental remediation: prospects and limitations, Water Air Soil Pollut., 223 (2012) 1363–1382.
[27] S.M. Ponder, J.G. Darab, J. Bucher, D. Caulder, I. Craig, L. Davis, N. Edelstein, W. Lukens, H. Nitsche, L.F. Rao, D.K. Shuh, T.E. Mallouk, Surface chemistry and electrochemistry of supported zerovalent iron nanoparticles in the remediation of aqueous metal contaminants, Chem. Mater., 13 (2001) 479–486.
[28] W. Stumm, J.J. Morgan, Aquatic Chemistry, 3rd ed., Wiley, New York, 1996.
[29] C.M. Wang, D.R. Baer, J.E. Amonette, M.H. Engelhard, J. Antony, Y. Qiang, Morphology and electronic structure of the oxide shell on the surface of iron nanoparticles, J. Am. Chem. Soc., 131(2009) 8824–8832.
[30] E.E. Carpenter, S. Calvin, R.M. Stroud, V.G. Harris, Passivated iron as core-shell nanoparticles, Chem. Mater., 15 (2003) 3245–3246.
[31] W. Liang, C. Dai, X. Zhou, Y. Zhang, Application of zero-valent iron nanoparticles for the removal of aqueous zinc ions under various experimental conditions, PLoS One, 9 (2014) 1–9.
[32] B.A. Balko, P.G. Tratnyek, Photoeffects on the reduction of carbon tetrachloride by zero-valent iron, J. Phys. Chem. B, 102 (1998) 1459–1465.
[33] A. Ausavasukhi, T. Sooknoi, Oxidation of tetrahydrofuran to butyrolactone catalyzed by iron-containing clay, Green Chem., 17 (2015) 435–441.
[34] A. Tabak, B. Afsin, B. Caglar, E. Koksal, Characterization and pillaring of a Turkish bentonite (Resadiye), J. Colloid Interface Sci., 313 (2007) 5–11.
[35] Z.-x. Chen, X.-y. Jin, Z.L. Chen, M. Megharaj, R. Naidu, Removal of methyl orange from aqueous solution using bentonite-supported nanoscale zero-valent iron, J. Colloid Interface Sci., 363 (2011) 601–607.
[36] Ç. Üzüm, T. Shahwan, A.E. Eroglu, K.R. Hallam, T.B. Scott, I. Lieberwirth, Synthesis and characterization of kaolinite-supported zero-valent iron nanoparticles and their application for the removal of aqueous Cu^{2+} and Co^{2+} ions, Appl. Clay Sci., 43 (2009) 172–181.
[37] X. Zhang, S. Lin, X.-Q. Lu, Z.-I. Chen, Removal of Pb(II) from water using synthesized kaolin supported nanoscale zero-valent iron, Chem. Eng. J., 163 (2010) 243–248.
[38] L.N. Shi, X. Zhang, Z.L. Chen, Removal of chromium (VI) from wastewater using bentonite-supported nanoscale zero-valent iron, Water Res., 45 (2011) 866–892.
[39] A.T. Sdiri, T. Higashi, F. Jamoussi, Adsorption of copper and zinc onto natural clay in single and binary systems, Int. J. Environ. Sci. Technol., 11 (2014) 1081–1092.
[40] T. Shahwan, Sorption kinetics: obtaining a pseudo-second order rate equation based on a mass balance approach, J. Environ. Chem. Eng., 2 (2014) 1001–1006.
[41] H. Kim, H.J. Hong, J. Jung, S.H. Kim, J.W. Yang, Degradation of trichloroethylene (TCE) by nanoscale zero-valent iron (nZVI) immobilized in alginate bead, J. Hazard. Mater., 176 (2010) 1038–1043.
[42] A. Afkhami, R. Moosavi, Adsorptive removal of Congo red, a carcinogenic textile dye, from aqueous solutions by maghemite nanoparticles, J. Hazard. Mater., 15 (2010) 398–403.
[43] R. Venkatapathy, D.G. Bessingpas, S. Canonica, J.A. Perlinger, Kinetic models for trichloroethylene transformation by zero-valent iron, Appl. Catal., B., 37 (2002) 139–159.
[44] M.H. Al-Jabari, S. Sulaiman, S. Ali, R. Barakat, A. Mubarak, S.A. Khan, Adsorption study of levofloxacin on reusable magnetic nanoparticles: kinetics and antibacterial activity, J. Mol. Liq., 291 (2019), doi: 10.1016/j.molliq.2019.111249.
[45] Z. Chia, Z. Wang, H. Chua, P. Bina, L. Lucian, Bentonite-supported nanoscale zero-valent iron granulated electrodes for industrial wastewater remediation, RSC Adv., 7 (2017) 44605–44613.
[46] M. Al-Jabari, I. Khalid, S. Sulaiman, I. Alawi, J. Shilo, Synthesis, characterization, kinetic and thermodynamic investigation of silica nanoparticles and their application in Mefenamic acid removal from aqueous solution, Desal. Wat. Treat., 129 (2018) 160–167.